Quarkonium Production at the LHC

R. Vogt

Nuclear Science Division, Lawrence Berkeley National Laboratory, Berkeley, CA 94720, USA

Physics Department, University of California, Davis, CA 95616, USA

Outline

- Total Cross Sections and Rapidity Distributions
- Initial and Final State Baseline Effects on J/ψ and Υ Production as a Function of y and Centrality
- Systems Studied: pp at 14, 9.9, 9.39, 9.27, 9, 8.8, 7, 6.3, 6.14, 5.84 and 5.5 TeV, pO at 9.9 and 7 TeV, pAr at 9.39 and 6.3 TeV, pKr at 9.27 and 6.14 TeV, pSn at 9 and 5.84 TeV, pPb at 8.8 and 5.5 TeV, O+O at 7 TeV, Ar+Ar at 6.3 TeV, Kr+Kr at 6.14 TeV, Sn+Sn at 5.84 TeV and Pb+Pb at 5.5 TeV

Production in Color Evaporation Model (CEM)

Gavai *et al.*, G. Schuler and R.V.

All quarkonium states are treated like $Q\overline{Q}$ below $H\overline{H}$ threshold

Distributions (x_F, p_T, $\sqrt{s}$, A) for all quarkonium family members identical — leads to constant ratios

At LO, $gg \to Q\overline{Q}$ and $q\overline{q} \to Q\overline{Q}$; NLO add $gq \to Q\overline{Q}q$

$$\sigma_C^{\rm CEM} = F_C \sum_{i,j} \int_{4m^2}^{4m_H^2} d\hat{s} \int dx_1 dx_2 \; f_{i/p}(x_1,\mu^2) \; f_{j/p}(x_2,\mu^2) \; \hat{\sigma}_{ij}(\hat{s}) \; \delta(\hat{s} - x_1 x_2 s)$$

F_C fixed at NLO from total cross section data as a function of $\sqrt{s}$, $\sigma(x_F > 0)$ for inclusive J/ψ and $B_{\mu\mu} d\sigma(\Upsilon + \Upsilon' + \Upsilon'')_{y=0}/dy$

Values of m and μ (here $\mu \propto \sqrt{(p_{T\,Q}^2 + p_{T\,\overline{Q}}^2)/2 + m_Q^2} = m_{T\,Q\overline{Q}} \equiv m_T$ in the exclusive $Q\overline{Q}$ code) for several parton densities fixed from $Q\overline{Q}$ production

We don't use NRQCD to study shadowing and absorption at LHC since total cross section matrix elements needed are fit to CTEQ3L (obsolete) parton densities – would need to refit matrix elements with more recent PDF set better behaved at low x

Production and Feed Down Fractions

Data and branching ratios can be used to separate out the F_C's for each state in quarkonium family

Resonance	$\sigma_i^{\rm dir}/\sigma_H$	f_i
J/ψ	**0.62**	**0.62**
ψ'	**0.14**	**0.08**
χ_{c1}	**0.6**	**0.16**
χ_{c2}	**0.99**	**0.14**
Υ	**0.52**	**0.52**
Υ'	**0.33**	**0.10**
Υ''	**0.20**	**0.02**
$\chi_b(1P)$	**1.08**	**0.26**
$\chi_b(2P)$	**0.84**	**0.10**

Table 1: The ratios of the direct quarkonium production cross sections, $\sigma_i^{\rm dir}$, to the inclusive J/ψ and Υ cross sections, denoted σ_H, and the feed down contributions of all states to the J/ψ and Υ cross sections, f_i.

Fitted Fractions and J/ψ Cross Sections in CEM

Case	PDF	m (GeV)	μ/m_T	$\sigma_{J/\psi}/\sigma_C^{\rm CEM}$
$\psi 1$	MRST HO	1.2	2	0.0144
$\psi 2$	MRST HO	1.4	1	0.0248
$\psi 3$	CTEQ 5M	1.2	2	0.0155
$\psi 4$	GRV 98 HO	1.3	1	0.0229

Table 2: The production fractions obtained from simultaneously fitting F_C to the J/ψ total cross sections and $y = 0$ cross sections as a function of energy. The PDF, charm quark mass, and scales used are obtained from comparison of the $c\overline{c}$ cross section to data.

Extrapolated J/ψ Total Cross Sections

Total forward J/ψ cross sections extrapolated to higher energy

Energy dependence obtained from NLO CEM

Factor of $\sim 1.6 - 2$ between results at 200 GeV and at 5.5 TeV

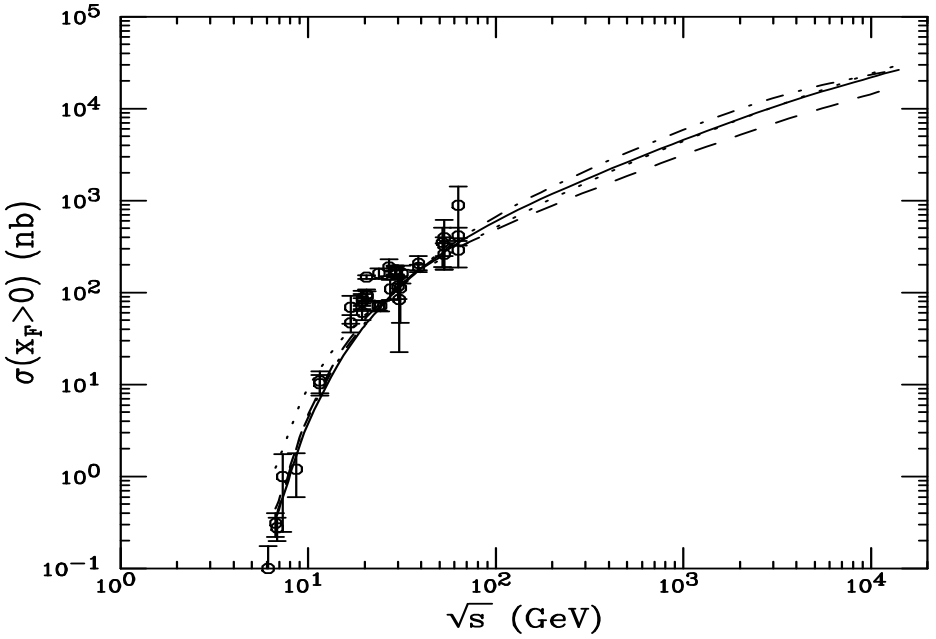

Figure 1: NLO J/ψ forward cross sections. The solid curve employs the MRST HO distributions with $m = 1.2$ GeV $\mu/m_T = 2$, the dashed, MRST HO with $m = 1.4$ GeV $\mu/m_T = 1$, the dot-dashed, CTEQ 5M with $m = 1.2$ GeV $\mu/m_T = 2$, and the dotted, GRV 98 HO with $m = 1.3$ GeV $\mu/m_T = 1$.

Charmonium Cross Sections in pp and AA in CEM

Direct quarkonium (per nucleon pair) and inclusive lepton pair (times A^2), including EKS98 shadowing

		$\sigma^{\rm dir}$/nucleon pair (μb)				$B\sigma^{\rm inc}A^2$ (μb)	
System	$\sqrt{s}$ (TeV)	$\sigma_{J/\psi}$	$\sigma_{\chi c1}$	$\sigma_{\chi c2}$	$\sigma_{\psi'}$	$\sigma_{J/\psi}$	$\sigma_{\psi'}$
pp	14	32.9	31.8	52.5	7.43	3.18	0.057
pp	8.8	25.0	24.2	39.9	5.65	2.42	0.044
pPb	8.8	19.5	18.9	31.1	4.40	392.3	7.05
pp	7	21.8	21.1	34.9	4.93	2.11	0.038
O+O	7	17.6	17.0	28.1	3.98	436.2	7.84
pp	6.3	20.5	19.9	32.8	4.63	1.99	0.036
Ar+Ar	6.3	15.0	14.5	23.9	3.38	2321	41.7
pp	6.14	20.2	19.6	32.3	4.56	1.96	0.035
Kr+Kr	6.14	13.7	13.2	21.8	3.08	9327	167.6
pp	5.84	19.6	19.0	31.3	4.42	1.90	0.034
Sn+Sn	5.84	12.8	12.4	20.4	2.89	17545	315.2
pp	5.5	18.9	18.3	30.2	4.26	1.83	0.033
Pb+Pb	5.5	11.7	11.3	18.7	2.64	48930	879

Table 3: The direct cross section per nucleon pair and the dilepton yield multiplied by A^2 for minimum bias. The result are given for several systems and pp is compared to pA and AA interactions. The case $\psi 1$, MRST with $m_c = 1.2$ GeV, $\mu = 2m_c$, is shown.

Fitted Fractions and Υ Cross Sections in CEM

Case	**PDF**	m **(GeV)**	μ/m_T	$\sigma_{B\Sigma\Upsilon}/\sigma_b^{\rm CEM}$	$\sigma_\Upsilon/\sigma_b^{\rm CEM}$
Υ1	**MRST HO**	**4.75**	**1**	**0.000963**	**0.0276**
Υ2	**MRST HO**	**4.50**	**2**	**0.000701**	**0.0201**
Υ3	**MRST HO**	**5.00**	**0.5**	**0.001766**	**0.0508**
Υ4	**GRV 98 HO**	**4.75**	**1**	**0.000787**	**0.0225**

Table 4: The production fractions obtained from fitting the CEM cross section to the combined Υ $y = 0$ cross sections to dimuons. The PDF, charm quark mass, and scales used are the same as those obtained by comparison of the $b\overline{b}$ cross section to data.

Inclusive Υ Cross Sections at $y = 0$

Cross sections include all $\Upsilon(nS)$ states and their decays to muon pairs

Data is from pp interactions except for highest two points where only $p\overline{p}$ colliders available

At high energies, $gg \to Q\overline{Q}$ dominates and differences between $p\overline{p} \to \Upsilon$ and $pp \to \Upsilon$ are negligible

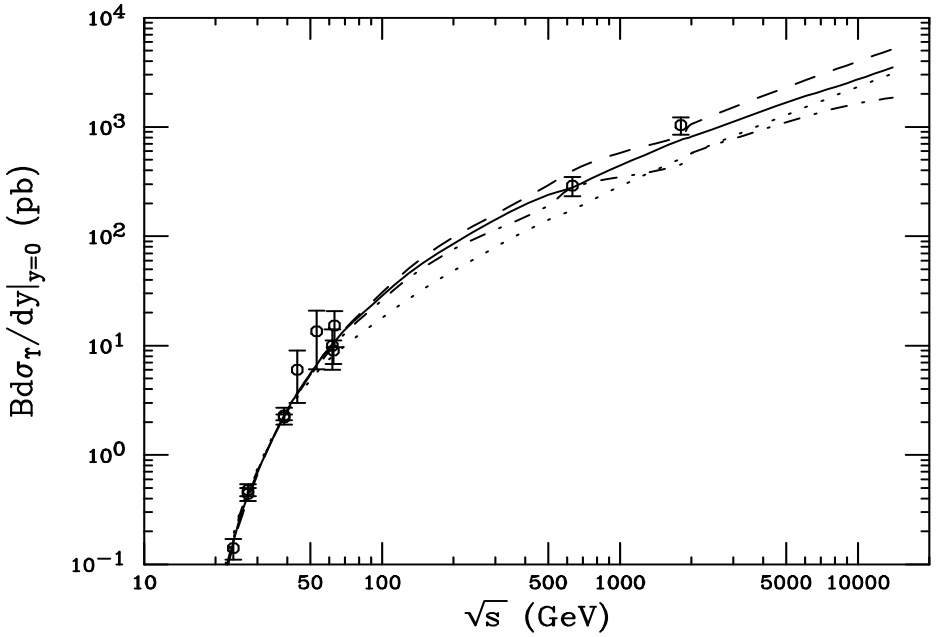

Figure 2: Inclusive Υ production data, combined from all three S states, and compared to NLO CEM calculations. The solid curve employs the MRST HO distributions with $m = 4.75$ GeV $\mu/m_T = 1$, the dashed, $m = 4.5$ GeV $\mu/m_T = 0.5$, the dot-dashed, $m = 5$ GeV $\mu/m_T = 2$, and the dotted, GRV 98 HO with $m = 4.75$ GeV $\mu/m_T = 1$.

Bottomonium Cross Sections in pp and AA in CEM

Direct quarkonium (per nucleon pair) and inclusive lepton pair (times A^2), including EKS98 shadowing

		$\sigma^{\rm dir}$/nucleon pair (μb)					$B\sigma^{\rm inc}A^2$ (μb)		
System	$\sqrt{s}$ **(TeV)**	σ_Υ	$\sigma_{\Upsilon'}$	$\sigma_{\Upsilon''}$	$\sigma_{\chi_b(1P)}$	$\sigma_{\chi_b(2P)}$	σ_Υ	$\sigma_{\Upsilon'}$	$\sigma_{\Upsilon''}$
pp	14	0.43	0.27	0.16	0.89	0.69	0.020	0.0050	0.0030
pp	8.8	0.29	0.18	0.11	0.60	0.47	0.014	0.0040	0.0020
pPb	8.8	0.25	0.16	0.097	0.52	0.41	2.51	0.65	0.37
pp	7	0.23	0.15	0.090	0.48	0.38	0.011	0.0029	0.0016
O+O	7	0.21	0.13	0.081	0.44	0.34	2.57	0.66	0.38
pp	6.3	0.21	0.14	0.082	0.44	0.34	0.010	0.0026	0.0015
Ar+Ar	6.3	0.18	0.12	0.070	0.38	0.29	13.8	3.59	2.02
pp	6.14	0.21	0.13	0.080	0.43	0.33	0.0099	0.0026	0.0014
Kr+Kr	6.14	0.17	0.11	0.066	0.35	0.28	57.4	14.8	8.38
pp	5.84	0.20	0.12	0.076	0.41	0.32	0.0094	0.0024	0.0014
Sn+Sn	5.84	0.16	0.10	0.062	0.33	0.26	108.1	28.0	15.8
pp	5.5	0.19	0.12	0.070	0.39	0.30	0.0090	0.0020	0.0013
Pb+Pb	5.5	0.15	0.094	0.057	0.31	0.24	304	78.8	44.4

Table 5: The direct cross section per nucleon pair and the dilepton yield multiplied by A^2 for minimum bias. The result are given for several systems and pp is compared to pA and AA interactions. The case Υ1, MRST with $m_b = 4.75$ GeV, $\mu = m_b$, is shown.

Average x_2 as a Function of Energy and Rapidity

Calculated in the CEM ($\langle x_1 \rangle$ is mirror imagine of $\langle x_2 \rangle$)

Increasing $\sqrt{S}$ broadens y, decreases x_2; go from ψ to Υ increases x_2

Red horizontal line indicates minimum x of recent PDFs: $x = 10^{-5}$

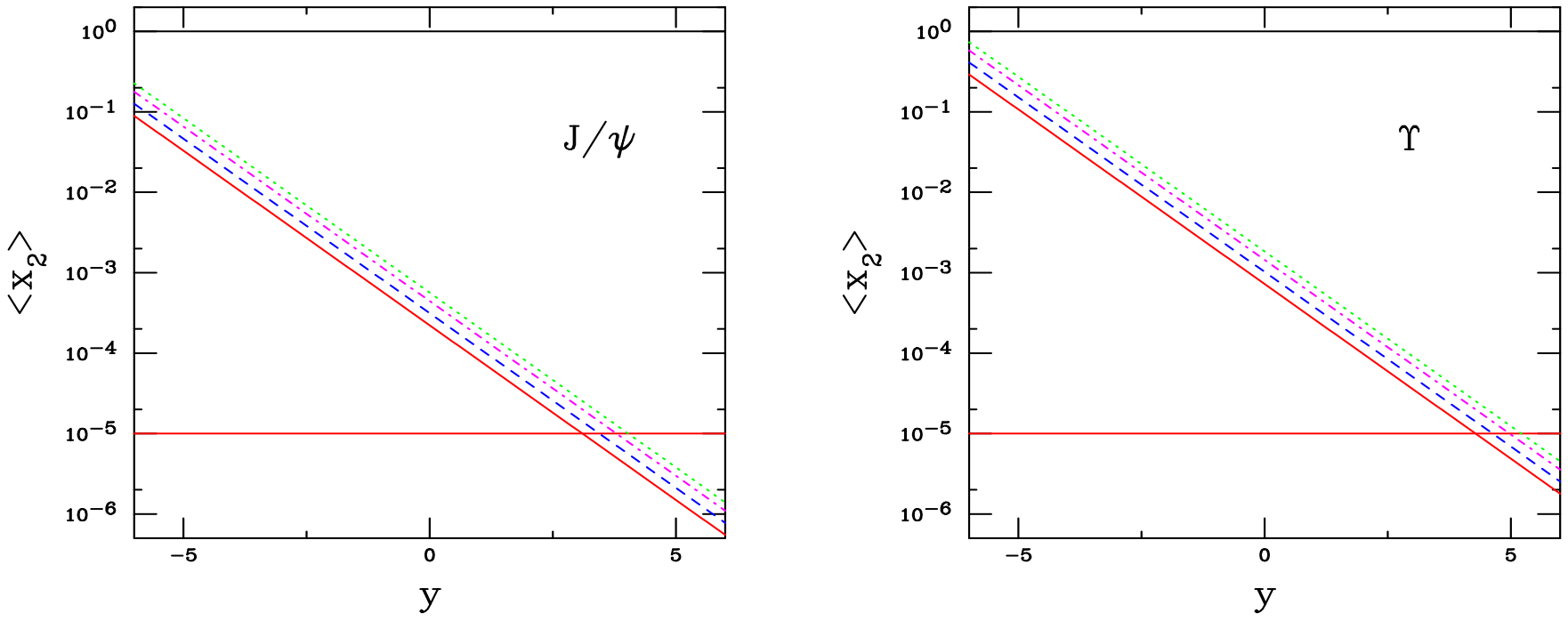

Figure 3: We give the average value of the nucleon momentum fraction, x_2, in pp collisions as a function of rapidity for J/ψ (left) and Υ (right) production at 14 (red), 9.9 (blue), 7 (magenta) and 5.5 (green) TeV. The red line indicates $x = 10^{-5}$.

Predictions of Quarkonia Rapidity Spectra at LHC

Use GRV98 PDFs since gluon density is better behaved for $x < 10^{-5}$
MRST and CTEQ distributions much flatter away from midrapidity since gluon distributions take their $x = 10^{-5}$ value for lower x

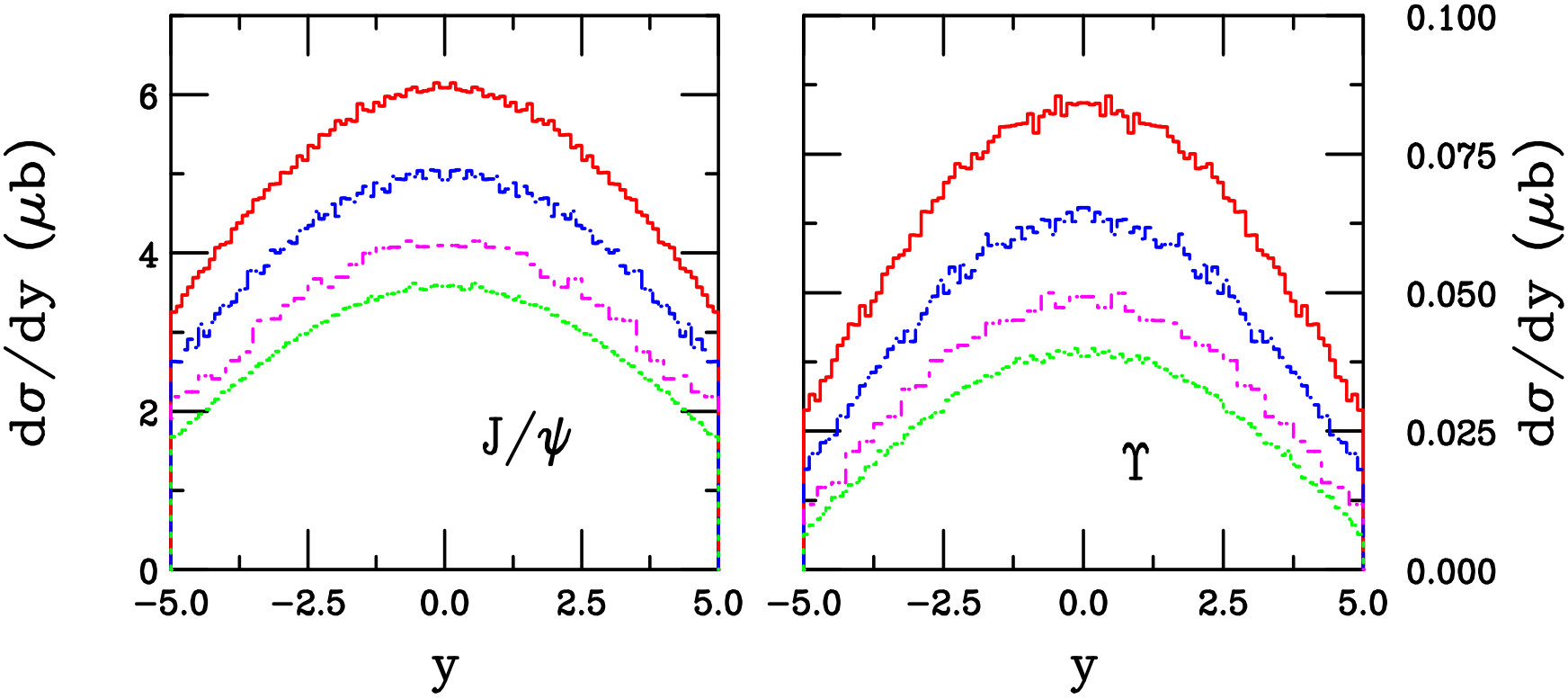

Figure 4: The inclusive J/ψ (left) and Υ (right) rapidity distributions, calculated for the GRV98 parton densities (cases $\psi 4$ and $\Upsilon 4$ for pp collisions at 14 (red), 9.9 (blue), 7 (magenta) and 5.5 (green) TeV respectively.

Prediction of J/ψ Rapidity Distributions at RHIC

Agreement of CEM calculation with overall normalization of Run 3 data good

Shape has right trend for d+Au with EKS98 shadowing

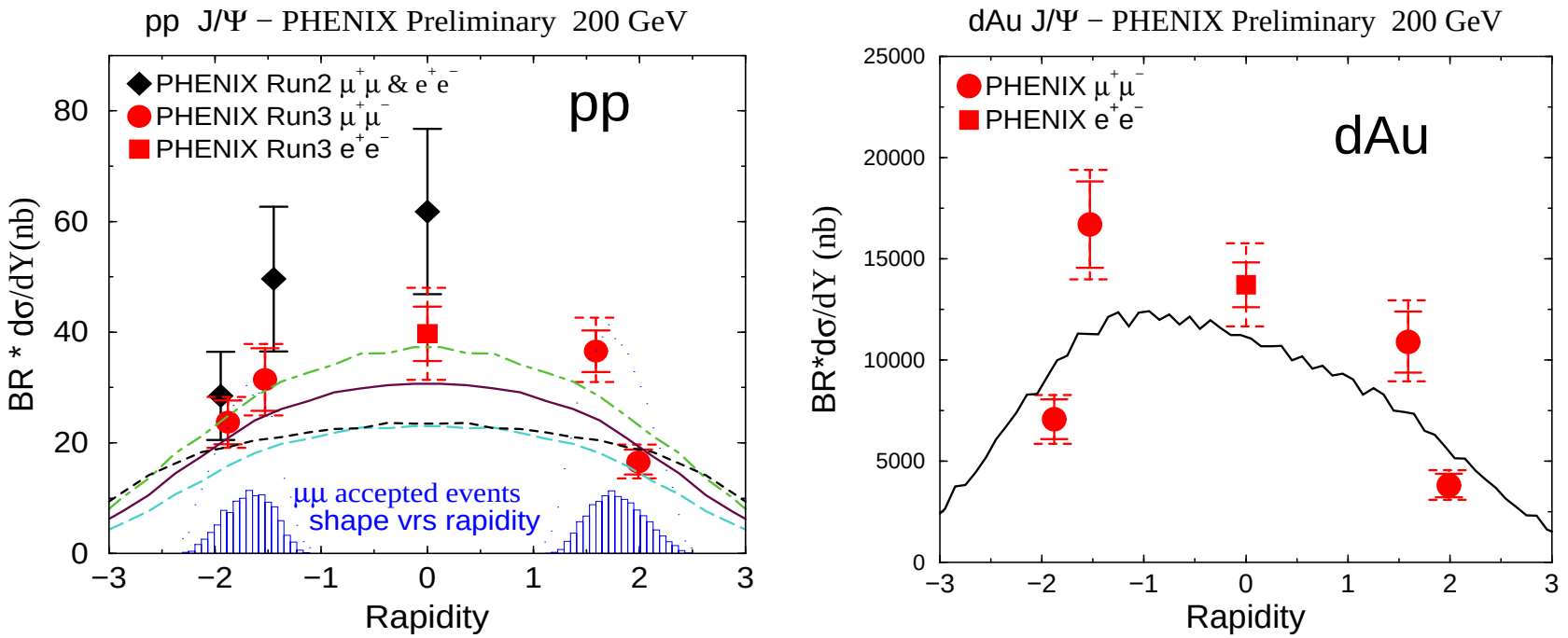

Figure 5: The inclusive J/ψ y distributions in $\sqrt{s} = 200$ pp (left-hand side for $\psi 1$ (solid), $\psi 2$ (dashed), $\psi 3$ (dot-dashed) and $\psi 4$ (dotted)) and d+Au (right-hand side with $\psi 1$ and EKS98). The rapidity distributions are unaffected by broadening. Thanks to Mike Leitch for making the plots!

Nuclear Effects on y Distributions Important in pA

Nuclear effects important in fixed-target charmonium production

In extrapolated pA cross sections, the exponent α ($\sigma_{pA} = \sigma_{pp}A^{\alpha}$) was shown to be a function of both x_F and p_T

Several mechanisms affect A dependence in cold matter, we consider two here:

- **Nuclear Shadowing — initial-state effect on the parton distributions affecting the level of production, important as a function of rapidity/x_F**
- **Absorption — final-state effect, after $c\overline{c}$ that forms the J/ψ has been produced, pair breaks up in matter due to interactions with nucleons**

Including shadowing for $\sqrt{S} \geq 38$ GeV makes $\alpha < 1$ for $x_F/y > 0$, hence reducing the absorption cross section needed

At high x_F, other mechanisms (energy loss, intrinsic charm) may be important but $x_F > 0.25$ corresponds to $y > 6$ at 5.5 TeV (larger y for higher $\sqrt{S}$) and will not appear in p_T-integrated y distributions

Nuclear Parton Distributions

Nuclear parton densities

$$F_i^A(x,Q^2,\vec{r},z) = \rho_A(s) S^i(A,x,Q^2,\vec{r},z) f_i^N(x,Q^2) s = \sqrt{b^2+z^2}$$
$$\rho_A(s) = \rho_0 \frac{1+\omega(s/R_A)^2}{1+\exp[(s-R_A)/d]}$$

We use EKS98, Frankfurt, Guzey and Strikman (FGSo, FGSh, and FGSl) and DeFlorian and Sassot (nDS and nDSg)

EKS98, FGSo, nDS and nDSg have no spatial dependence, FGSh and FGSl do

With no nuclear modifications, $S^i(A,x,Q^2,\vec{r},z) \equiv 1$

Spatial depndence proportional to nuclear path length:

$$S_\rho^i(A,x,Q^2,\vec{r},z) = 1 + N_\rho(S^i(A,x,Q^2)-1)\frac{\int dz \rho_A(\vec{r},z)}{\int dz \rho_A(0,z)}$$

Normalization: $(1/A)\int d^2r dz \rho_A(s) S_\rho^i \equiv S^i$**. Larger than average modifications for** $b=0$**. Nucleons like free protons when** $s \gg R_A$**. Similar normalization for FGS inhomogeneous parameterizations.**

Comparing Shadowing Parameterizations: x Dependence

EKS98, nDS and nDSg for all A, FGS available for $A = 12, 40, 110$ and 197/206, use $A = 12$ for O and $A = 110$ for Kr and Sn with them

Ratios shown for GRV98 scales, $\mu = 1.3$ and 4.75 GeV for charm and bottom but if $\mu < \mu_0$ for set, take $\mu = \mu_0$

EKS98 and nDSg similar for $A = 208$ but quite different for smaller A

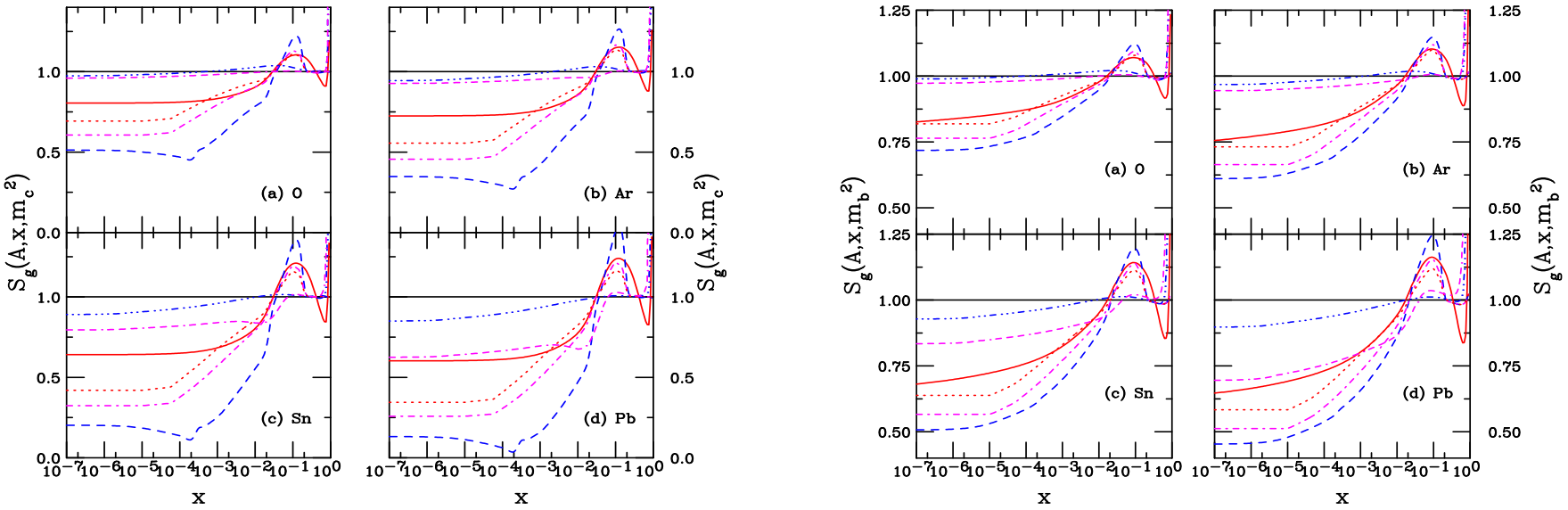

Figure 6: Shadowing parameterizations for J/ψ (left) and Υ (right) scales for C (upper left), Ar (upper right), Sn (lower left) and Pb (lower right) nuclei. The parameterizations are EKS98 (solid red), FGSo (dashed blue), FGSh (dot-dashed magenta), FGSl (dotted red), nDS (dot-dot-dot-dashed blue) and nDSg (dash-dash-dash dotted magenta).

J/ψ Absorption by Nucleons

Woods-Saxon nuclear density profiles typically used

$$\begin{aligned}\sigma_{pA} &= \sigma_{pN} \int d^2b \int_{-\infty}^{\infty} dz\, \rho_A(b,z) S_A^{\rm abs}(b) \\ &= \sigma_{pN} \int d^2b \int_{-\infty}^{\infty} dz\, \rho_A(b,z) \exp\left\{-\int_z^{\infty} dz' \rho_A(b,z') \sigma_{\rm abs}(z'-z)\right\}\end{aligned}$$

Note that if $\rho_A = \rho_0$, $\alpha = 1 - 9\sigma_{\rm abs}/(16\pi r_0^2)$

Absorption Models

singlet Individual charmonium cross sections grow quadratically with proper time until formation time; only effective when state can form in target

octet $|(c\bar{c})_8 g\rangle$ state travels through nucleus, only forms charmonium outside; assume either "constant" over all y or "growing", allows octet to singlet conversion inside target at negative y – little difference at collider energy

NRQCD Nonrelativistic QCD approach differs from CEM in that states are produced with fixed singlet and octet contributions (J/ψ and ψ' predominantly octet, χ_c singlet so separate pA measurements should distinguish differences in absorption)

Here results only shown for CEM and constant octet absorption; at LHC energies singlet equivalent to no absorption in $|y| \leq 6$, growing and constant octet also equivalent and NRQCD matrix elements fit to obsolete CTEQ3L

Absorption and Shadowing at RHIC: Shadowing

EKS98 and FGS compared to RHIC d+Au data with 3 mb absorption cross section and MRST parton densities with $m = 1.2$ GeV, $\mu = 2m$

Lower scale GRV98 PDFs increases shadowing effect somewhat

Work with Mike Leitch suggests EKS98 and nDSg give best fit to RHIC data with $\sigma_{\rm abs} < 2$ mb

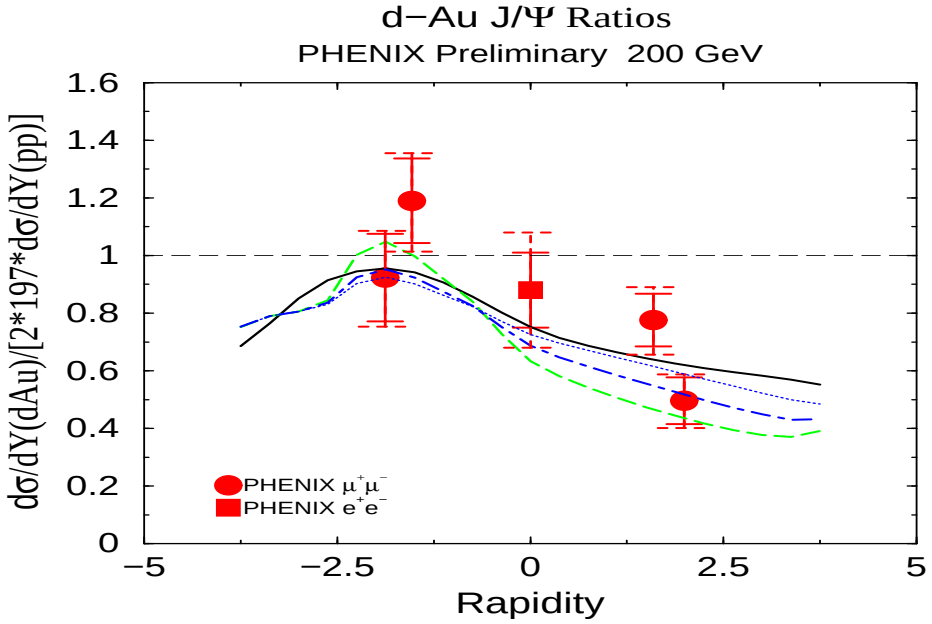

Figure 7: Comparison of the results for a 3 mb growing octet absorption cross section with the EKS98 (solid), FGSo (dashed), FGSh (dot-dashed) and FGSl (dotted) shadowing parameterizations. Thanks to Mike Leitch for making this plot!

J/ψ Absorption and Shadowing in pPb at 8.8 TeV

Left side: Effect of $\sigma_{\rm abs}$ is shown for various absorption models

Right side: Comparing shadowing parameterizations for $\sigma_{\rm abs} = 2$ mb

Absorption a small effect relative to shadowing

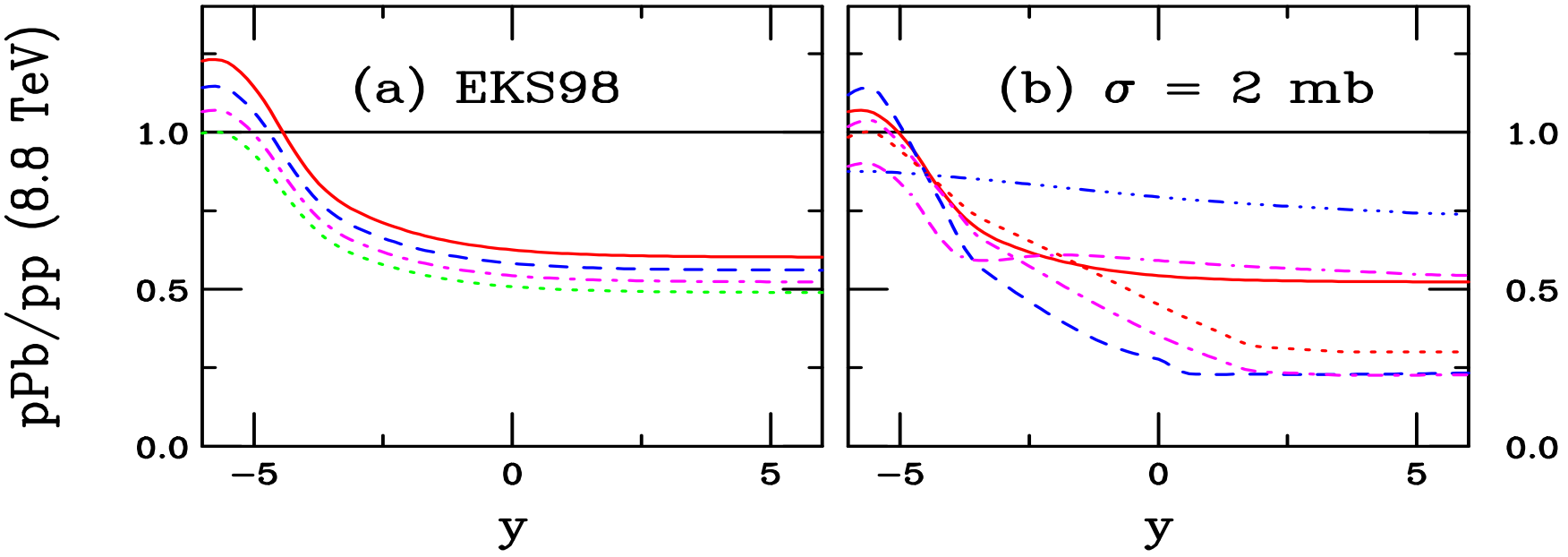

Figure 8: Left-hand side: The J/ψ pPb/pp ratio at 8.8 TeV with the EKS98 shadowing parameterization for $\sigma_{\rm abs} = 0$ (solid red), 1 (dashed blue), 2 (dot-dashed magneta) and 3 (dotted green) mb. Right-hand side: Comparison of shadowing results for a 2 mb octet cross section with EKS98 (solid red), FGSo (dashed blue), FGSh (dot-dashed magenta), FGSl (dotted red), nDS (dot-dot-dot-dashed blue) and nDSg (dash-dash-dash-dotted magenta).

J/ψ Absorption and Shadowing in pPb at 5.5 TeV

Left side: Effect of $\sigma_{\rm abs}$ is shown for various absorption models

Right side: Comparing shadowing parameterizations for $\sigma_{\rm abs} = 2$ mb

Larger x values at smaller $\sqrt{S}$ moves antishadowing peak to larger y

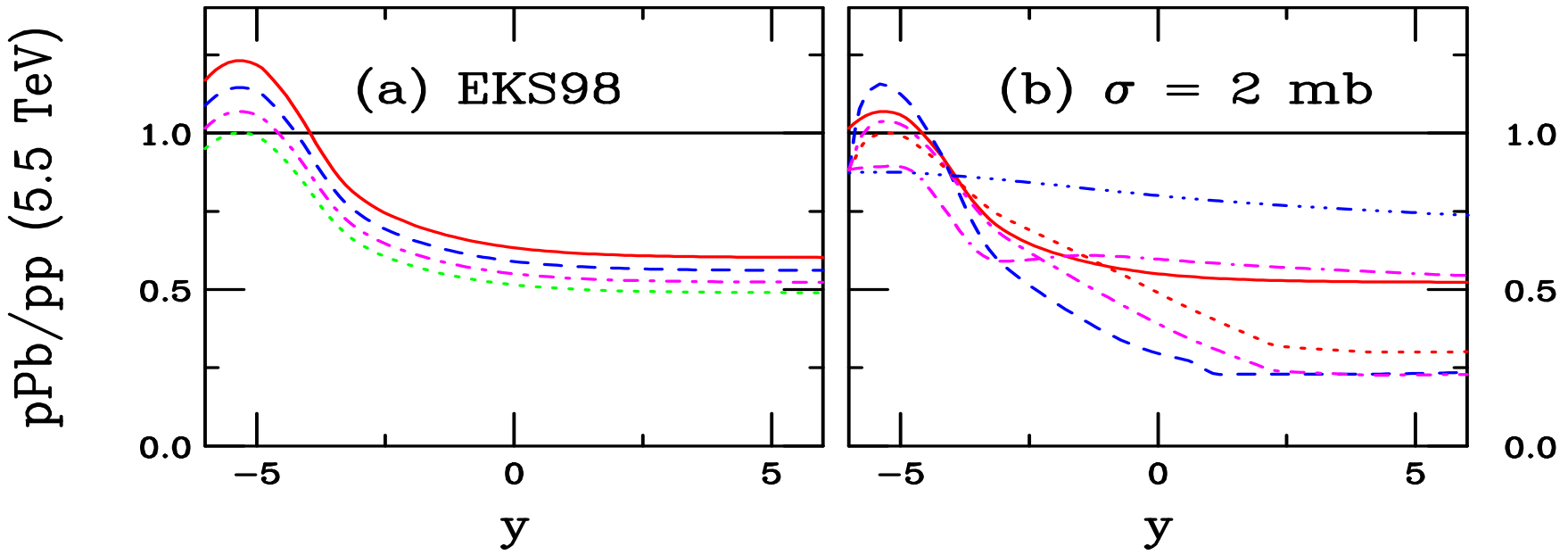

Figure 9: Left-hand side: The J/ψ pPb/pp ratio at 5.5 TeV with the EKS98 shadowing parameterization for $\sigma_{\rm abs} = 0$ (solid red), 1 (dashed blue), 2 (dot-dashed magneta) and 3 (dotted green) mb. Right-hand side: Comparison of shadowing results for a 2 mb octet cross section with EKS98 (solid red), FGSo (dashed blue), FGSh (dot-dashed magenta), FGSl (dotted red), nDS (dot-dot-dot-dashed blue) and nDSg (dash-dash-dash-dotted magenta).

J/ψ Absorption and Shadowing in Pb+Pb at 5.5 TeV

Left side: Effect of $\sigma_{\rm abs}$ is shown for various absorption models

Right side: Comparing shadowing parameterizations for $\sigma_{\rm abs} = 2$ mb

Two nuclei produces two antishadowing peaks with dip in between

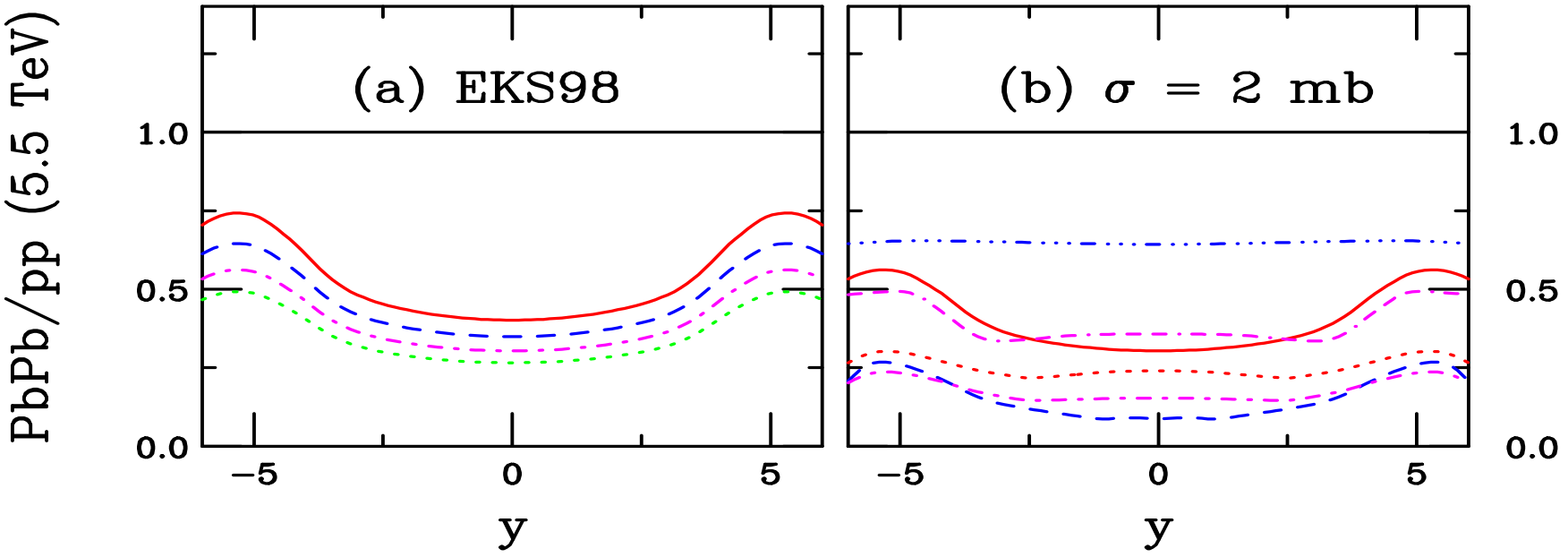

Figure 10: Left-hand side: The J/ψ Pb+Pb/pp ratio at 5.5 TeV with the EKS98 shadowing parameterization for $\sigma_{\rm abs} = 0$ (solid red), 1 (dashed blue), 2 (dot-dashed magneta) and 3 (dotted green) mb. Right-hand side: Comparison of shadowing results for a 2 mb octet cross section with EKS98 (solid red), FGSo (dashed blue), FGSh (dot-dashed magenta), FGSl (dotted red), nDS (dot-dot-dot-dashed blue) and nDSg (dash-dash-dash-dotted magenta).

J/ψ Absorption and Shadowing in pA

Left: Ratio for pA at given $\sqrt{S}$ relative to pp at 14 TeV, most likely baseline, does not significantly change shape

Right: pA/pp at same $\sqrt{S}$, effect of increasing A greater than changing energy – No rapidity shift assumed either case

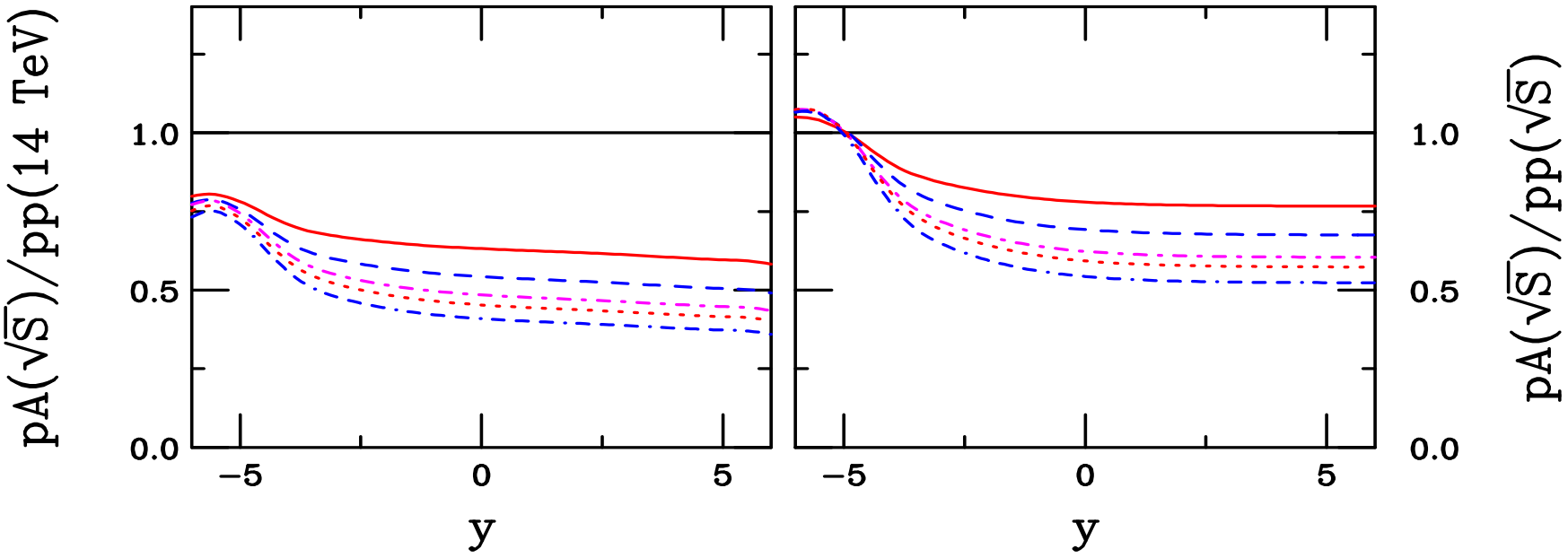

Figure 11: The J/ψ pA/pp ratio for pA at nominal energy relative to pp at 14 TeV (left-hand side) and for pA and pp at the same energy (right hand side) with the EKS98 parameterization and $\sigma_{\rm abs} = 2$ mb. The curves are pO at 9.9 TeV (solid red), pAr at 9.39 TeV (dashed blue), pKr at 9.27 TeV (dot-dashed magenta), pSn at 9 TeV (dotted red) and pPb at 8.8 TeV (dash-dash-dash-dotted blue).

Real pA Collisions Have Rapidity Shift

Proton beam has energy of 7 TeV

Ion beams have energy of $7Z/A$ so the more neutrons, the less energetic the ion beam

AA and tuned pp collisions have same energy in both beams but in pA, the center of mass rapidity is shifted, shift increases with A

A	E_A (TeV)	$\sqrt{S_{NN}}$ (TeV)	y_A	$y_p - y_A$	$\Delta y_{\rm cm}$
O	**3.5**	**9.9**	**8.92**	**0.690**	**0.345**
Ar	**3.15**	**9.39**	**8.81**	**0.798**	**0.399**
Kr	**3.07**	**9.27**	**8.79**	**0.824**	**0.412**
Sn	**2.92**	**9.0**	**8.74**	**0.874**	**0.437**
Pb	**2.75**	**8.8**	**8.67**	**0.934**	**0.467**

Table 6: For each ion species at the LHC, the maximum beam energy, the corresponding $\sqrt{S_{NN}} = \sqrt{4E_pE_A}$ with $E_p = 7$ TeV, the maximum ion rapidity ($y_p = 9.61$), the rapidity difference, $y_p - y_A$, and the center of mass rapidity shift is given.

J/ψ Absorption and Shadowing in Realistic pA

Rapidity shift included for both cases

Left: Shifted pA relative to pp at 14 TeV, flatter than with no shift

Right: pA/pp at same $\sqrt{S_{NN}}$, antishadowing peak visible

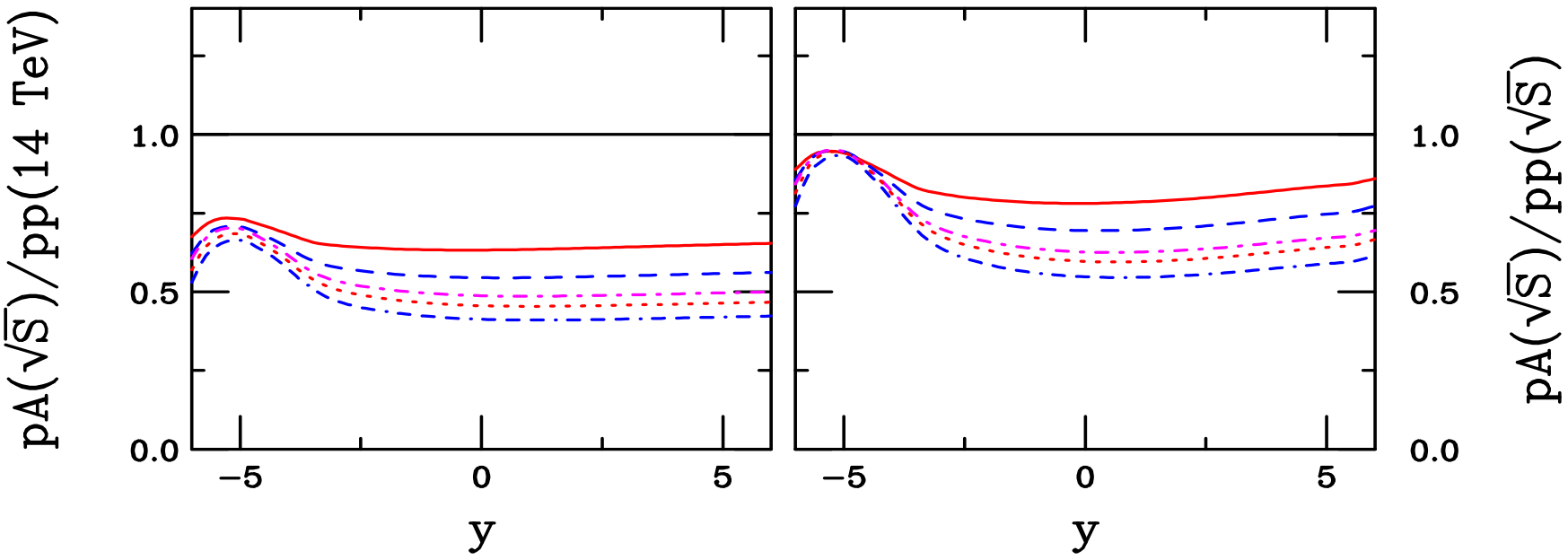

Figure 12: The J/ψ pA/pp ratio for pA at nominal energy relative to pp at 14 TeV (left-hand side) and for pA and pp at the same energy (right hand side) with the EKS98 parameterization and $\sigma_{\rm abs} = 2$ mb. The curves are pO at 9.9 TeV (solid red), pAr at 9.39 TeV (dashed blue), pKr at 9.27 TeV (dot-dashed magenta), pSn at 9 TeV (dotted red) and pPb at 8.8 TeV (dash-dash-dash-dotted blue). The rapidity shift in pA is now included.

J/ψ Absorption and Shadowing in AA

Left: Ratio for AA at given $\sqrt{S}$ relative to pp at 14 TeV, most likely baseline, flatter but similar shape

Right: AA/pp at same $\sqrt{S}$, effect of increasing A greater than changing energy

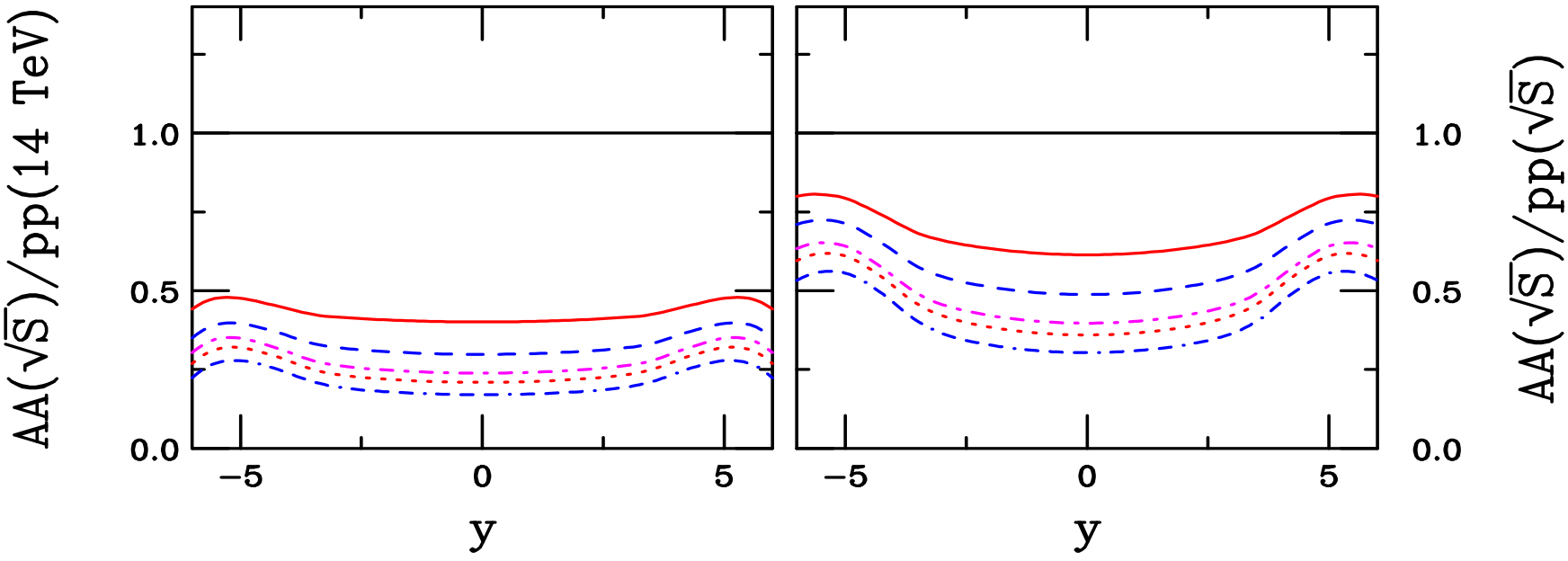

Figure 13: The J/ψ AA/pp ratio for AA at nominal energy relative to pp at 14 TeV (left-hand side) and for AA and pp at the same energy (right hand side) with the EKS98 parameterization and $\sigma_{\rm abs} = 2$ mb. The curves are O+O at 7 TeV (solid red), Ar+Ar at 6.3 TeV (dashed blue), Kr+Kr at 6.14 TeV (dot-dashed magenta), Sn+Sn at 5.84 TeV (dotted red) and Pb+Pb at 5.5 TeV (dash-dash-dash-dotted blue).

Υ Absorption and Shadowing in pPb at 8.8 TeV

Left: Effect of $\sigma_{\rm abs}$ is shown for various absorption models

Right: Different shadowing for $\sigma_{\rm abs} = 1$ mb (lower cross section because Υ is smaller)

Antishadowing at larger y for Υ

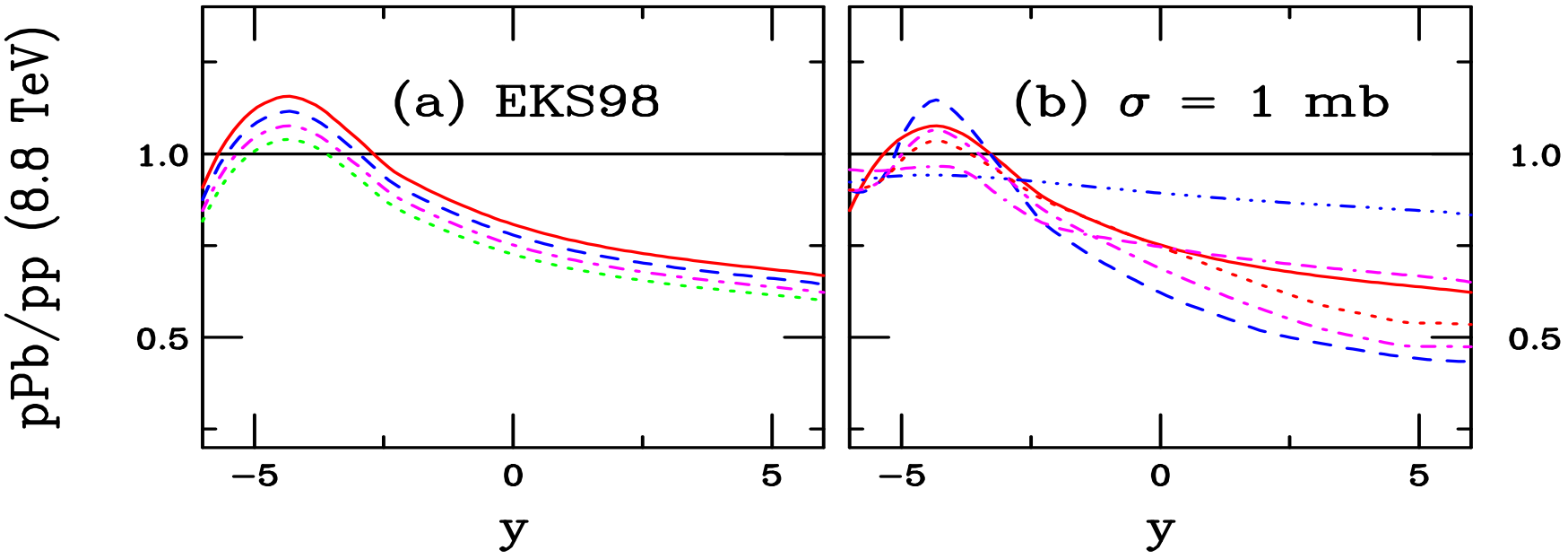

Figure 14: Left-hand side: The Υ pPb/pp ratio at 8.8 TeV with the EKS98 shadowing parameterization for $\sigma_{\rm abs} = 0$ (solid red), 0.5 (dashed blue), 1 (dot-dashed magneta) and 1.5 (dotted green) mb. Right-hand side: Comparison of shadowing results for a 1 mb octet cross section with EKS98 (solid red), FGSo (dashed blue), FGSh (dot-dashed magenta), FGSl (dotted red), nDS (dot-dot-dot-dashed blue) and nDSg (dash-dash-dash-dotted magenta).

Υ Absorption and Shadowing in pPb at 5.5 TeV

Left side: Effect of $\sigma_{\rm abs}$ is shown for various absorption models

Right side: Comparing shadowing parameterizations for $\sigma_{\rm abs} = 1$ mb

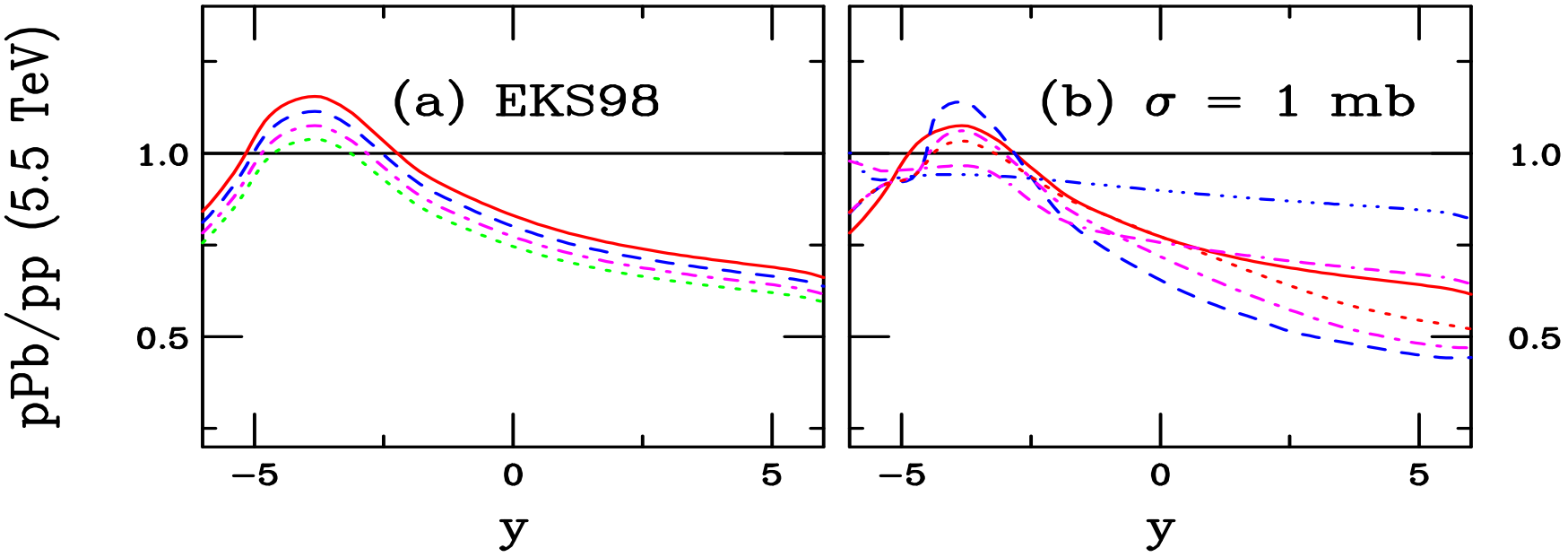

Figure 15: Left-hand side: The Υ pPb/pp ratio at 5.5 TeV with the EKS98 shadowing parameterization for $\sigma_{\rm abs} = 0$ (solid red), 0.5 (dashed blue), 1 (dot-dashed magneta) and 1.5 (dotted green) mb. Right-hand side: Comparison of shadowing results for a 1 mb octet cross section with EKS98 (solid red), FGSo (dashed blue), FGSh (dot-dashed magenta), FGSl (dotted red), nDS (dot-dot-dot-dashed blue) and nDSg (dash-dash-dash-dotted magenta).

Υ Absorption and Shadowing in Pb+Pb at 5.5 TeV

Left: Effect of $\sigma_{\rm abs}$ is shown for various absorption models

Right: Comparing shadowing parameterizations for $\sigma_{\rm abs} = 1$ mb

Two nuclei makes two antishadowing peaks with dip in between but peaks are closer than for J/ψ

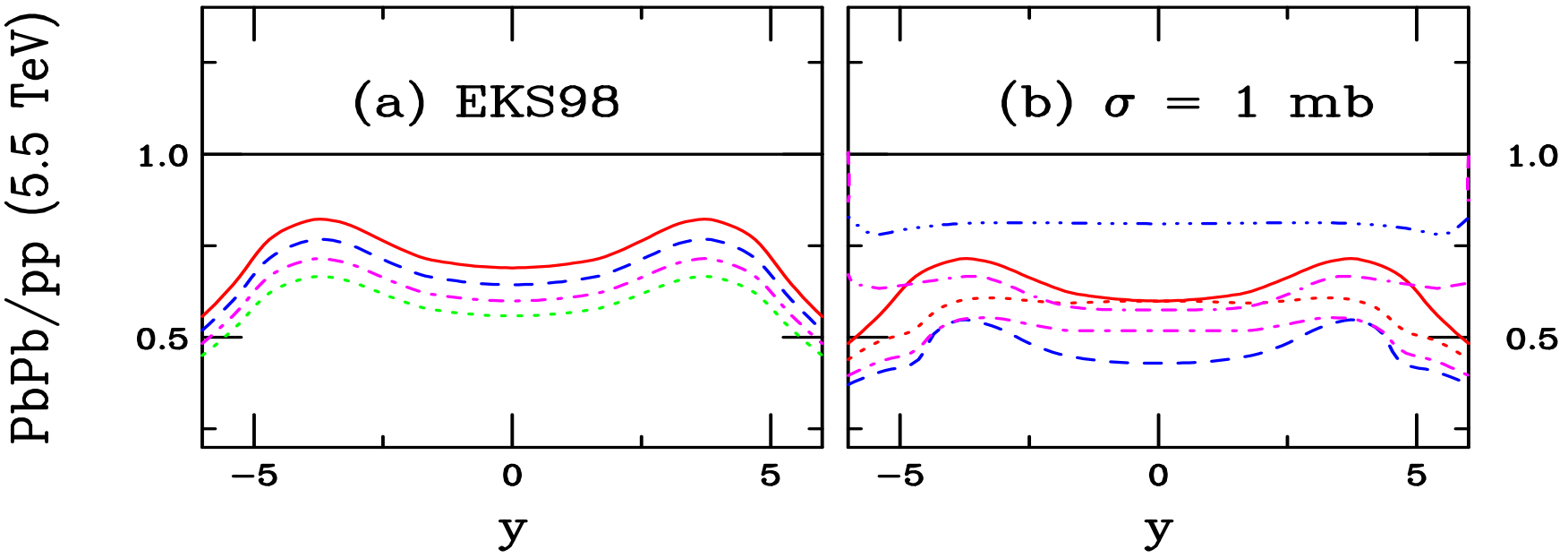

Figure 16: Left-hand side: The Υ Pb+Pb/pp ratio at 5.5 TeV with the EKS98 shadowing parameterization for $\sigma_{\rm abs} = 0$ (solid red), 0.5 (dashed blue), 1 (dot-dashed magneta) and 1.5 (dotted green) mb. Right-hand side: Comparison of shadowing results for a 1 mb octet cross section with EKS98 (solid red), FGSo (dashed blue), FGSh (dot-dashed magenta), FGSl (dotted red), nDS (dot-dot-dot-dashed blue) and nDSg (dash-dash-dash-dotted magenta).

Υ Absorption and Shadowing in pA

Left: Ratio for pA at given $\sqrt{S}$ relative to pp at 14 TeV, most likely baseline, turnover because y distribution narrower at lower $\sqrt{S}$

Right: pA/pp at same $\sqrt{S}$, effect of increasing A greater than changing energy

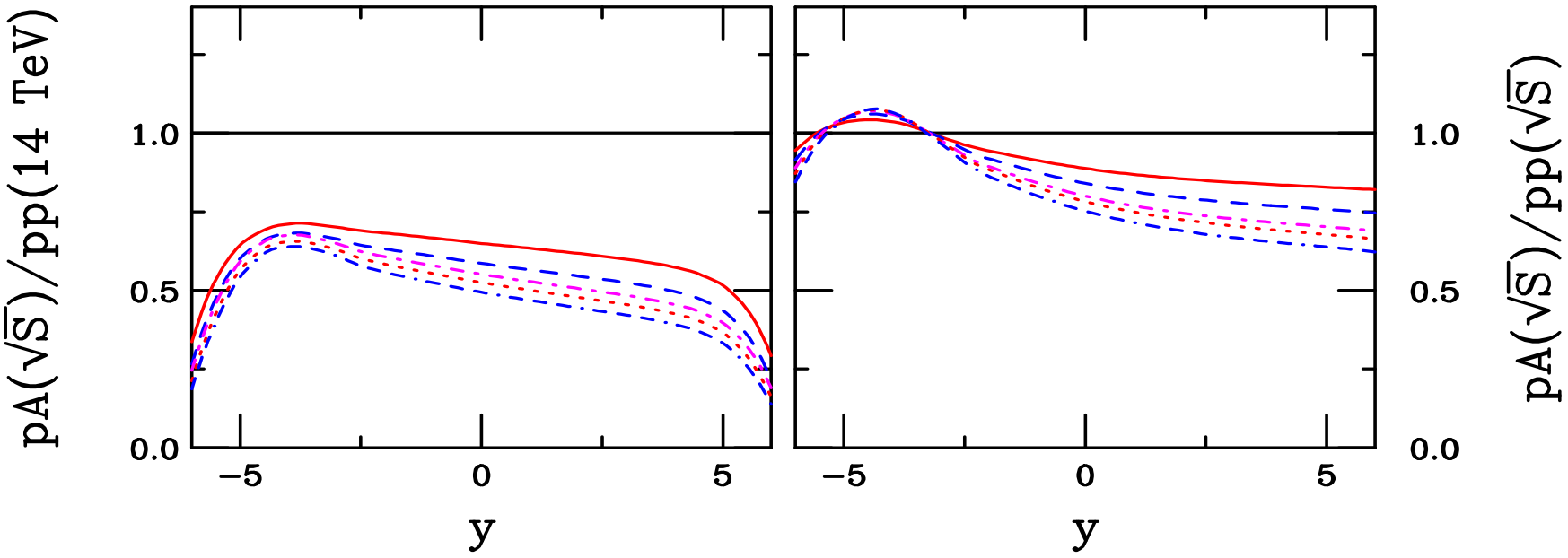

Figure 17: The Υ pA/pp ratio for pA at nominal energy relative to pp at 14 TeV (left-hand side) and for pA and pp at the same energy (right hand side) with the EKS98 parameterization and $\sigma_{\rm abs} = 1$ mb. The curves are pO at 9.9 TeV (solid red), pAr at 9.39 TeV (dashed blue), pKr at 9.27 TeV (dot-dashed magenta), pSn at 9 TeV (dotted red) and pPb at 8.8 TeV (dash-dash-dash-dotted blue).

Υ Absorption and Shadowing in Realistic pA

Rapidity shift now included

Left: Shifted pA relative to pp at 14 TeV, flatter than unshifted

Right: pA/pp at same $\sqrt{S}$, shift changes ratio

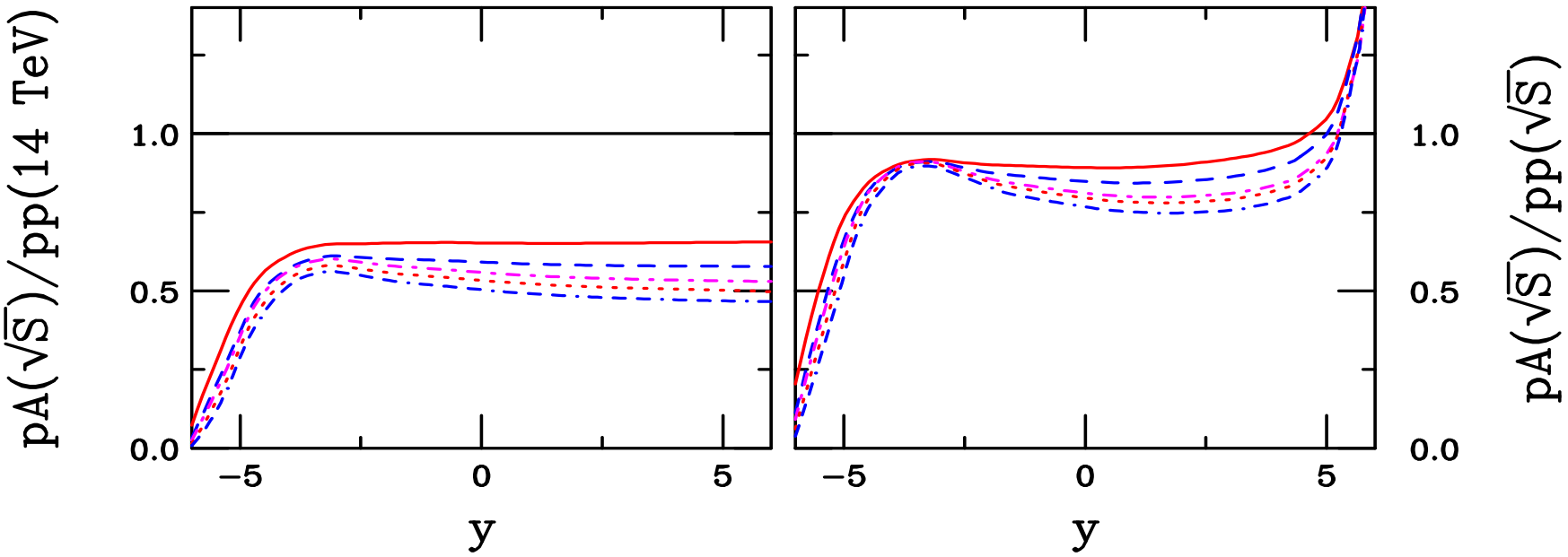

Figure 18: The Υ pA/pp ratio for pA at nominal energy relative to pp at 14 TeV (left-hand side) and for pA and pp at the same energy (right hand side) with the EKS98 parameterization and $\sigma_{\rm abs} = 1$ mb. The curves are pO at 9.9 TeV (solid red), pAr at 9.39 TeV (dashed blue), pKr at 9.27 TeV (dot-dashed magenta), pSn at 9 TeV (dotted red) and pPb at 8.8 TeV (dash-dash-dash-dotted blue). The rapidity shift is now included.

Υ Absorption and Shadowing in AA

Left: Ratio for AA at given $\sqrt{S}$ relative to pp at 14 TeV, most likely baseline

Right: AA/pp at same $\sqrt{S}$, effect of increasing A greater than changing energy

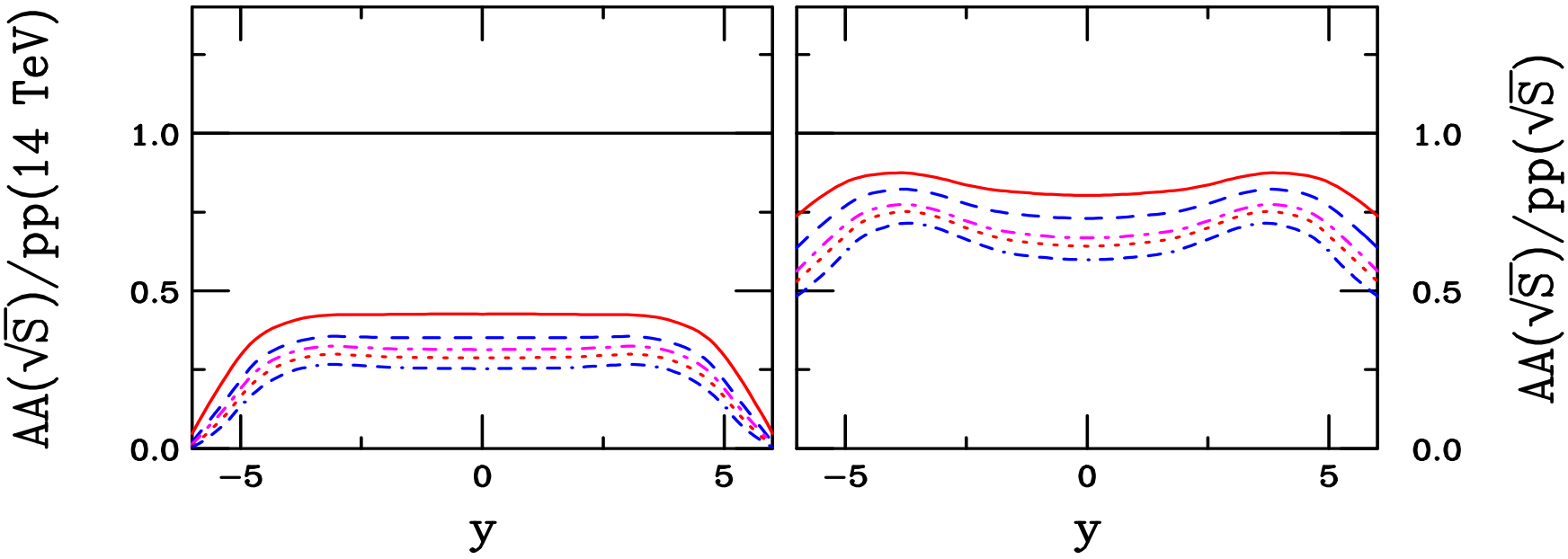

Figure 19: The Υ AA/pp ratio for AA at nominal energy relative to pp at 14 TeV (left-hand side) and for AA and pp at the same energy (right hand side) with the EKS98 parameterization and $\sigma_{\rm abs} = 1$ mb. The curves are O+O at 7 TeV (solid red), Ar+Ar at 6.3 TeV (dashed blue), Kr+Kr at 6.14 TeV (dot-dashed magenta), Sn+Sn at 5.84 TeV (dotted red) and Pb+Pb at 5.5 TeV (dash-dash-dash-dotted blue).

Inhomogeneous J/ψ Shadowing and Absorption

PHENIX results given as a function of $N_{\rm coll}$, the convolution of nuclear profile functions multiplied by the inelastic NN cross section

$$N_{\rm coll}(b) = \sigma_{NN}^{\rm in} \int d^2s T_A(s) T_B(|\vec{b} - \vec{s}|)$$

LHC Pb+Pb results presented as a function of $N_{\rm coll}$ for several rapidities: 0, 2 and 4 for EKS98 and nDSg parameterizations

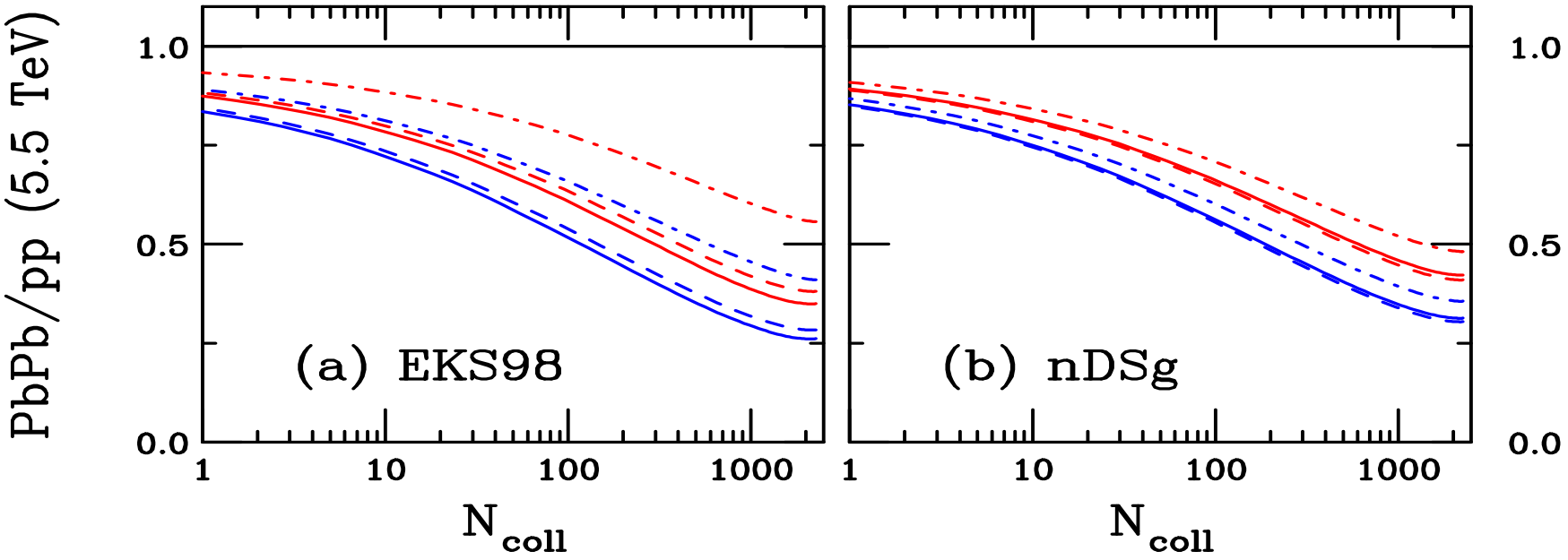

Figure 20: The J/ψ Pb+Pb/pp ratio as a function of $N_{\rm coll}$. The results are shown for $\sigma_{\rm abs} = 0$ (red) and 2 (blue) mb at $y = 0$ (solid), 2 (dashed) and 4 (dot-dashed). The EKS98 (left) and nDSg (right) parameterizations are compared.

Inhomogeneous Υ Shadowing and Absorption

LHC Pb+Pb results presented as a function of $N_{\rm coll}$ for several rapidities: 0, 2 and 4 for EKS98 and nDSg parameterizations

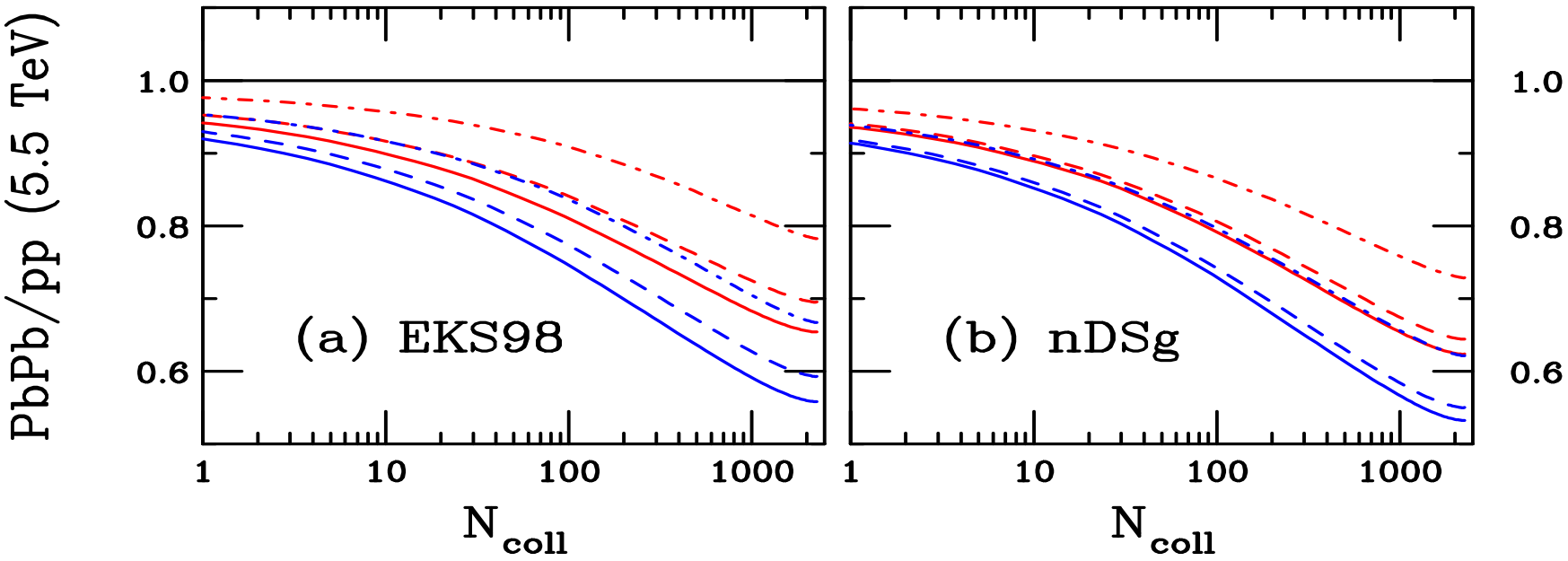

Figure 21: The Υ Pb+Pb/pp ratio as a function of $N_{\rm coll}$. The results are shown for $\sigma_{\rm abs} = 0$ (red) and 1 (blue) mb at $y = 0$ (solid), 2 (dashed) and 4 (dot-dashed). The EKS98 (left) and nDSg (right) parameterizations are compared.

Summary

- Results only shown for inclusive J/ψ and Υ but pp and pA measurements of χ_c, ψ', χ_b, Υ' and Υ'' should be possible at the LHC with similar pp distributions, χ absorption should be different – check production and absorption mechanisms
- Nuclear modification in d+Au relative to pp interactions at 200 GeV consistent with predictions of nuclear shadowing parameterizations with small absorption by nucleons
- ALICE needs to run both pA and Ap to study nuclear modification as a function of rapidity
- Comparison to pp at 14 TeV instead of pp at the same energy does not wash out shadowing and absorption effects
- pA interactions at more than one A may be necessary to distinguish between shadowing models
- High LHC energies provide exciting opportunity to measure low x parton densities at moderate to high Q^2